Chapter 16

Phonon Scattering and Electron Transport in Single Wall Carbon Nanotube

Bo Xu, Jiang Yin and Zhiguo Liu

Additional information is available at the end of the chapter

http://dx.doi.org/10.5772/51451

1. Introduction

Single-walled carbon nanotube (SWCNTs) can be thought of as graphene a single graphene sheet wrapped up to form a one-atom-thick cylinders. CNTs were discovered by Iijima [1] in 1991, since then the excellent charge transport properties of CNTs have been of great interest, for its great potential applications in nanoelectronics, such as high-speed field-effect transistors (FETs) [2, 3], single-electron memories [4], and chemical sensors [5]. The CNT has an atomic and electronic structure that gives it unique advantage as an FET channel. The band gap of the semiconducting SWCNT is inversely proportional to the tube diameter, which allows such tubes to be used in various different applications. CNTs display outstanding electrical properties such as ballistic transport or diffusive transport with long mean free path, which is of the order of a micrometer. Ballistic transport in CNTs has been experimentally demonstrated for low-bias conditions at low temperatures [6, 7]. High-performance CNT transistors operating close to the ballistic limit have also been reported [8-10]. Besides, one of the most important advantages is the CNT's excellent transport properties due to the high carrier mobility. The experimentally obtained carrier mobilities are of the orders 10^4 cm^2/Vs [11, 12] so exceptional device characteristics can indeed be expected. Current transport in long metallic CNTs, however, is found to saturate at ~ 25 μA at high biases, and the saturation mechanism is attributed to phonon scattering [13]. On the other hand, for short length metallic tubes, the current is found not to saturate but to increase well beyond the above limit [14, 15].

Nevertheless, carrier transport in these shorter tubes is still influenced by phonon scattering, and warrants a detailed physical understating of the scattering mechanisms due to its implications on device characteristics for both metallic as well as semiconducting CNTs. And there have been many theoretical studies on the calculation of carrier scattering rates and

mobilities in CNTs using semiclassical transport simulation based on the Boltzmann equation [16-22]. Similarly, phonon mode calculations for CNTs are also performed with varying degrees of complexity: continuum and forceconstant models [23-25] to first-principles based methods [26-28]. The determination of electron-phonon coupling strength is performed by using tight binding calculations [29-31] as well as first-principles techniques [32]. Non-equilibrium Green's function formalism also has been employed to treat the effects of phonon scattering in CNT [33-35].

In this work, we will show our physical simulation on the carrier mobilities under acoustic phonon scattering process. This work is organized as follows. In section II, we start with the basic properties of CNTs. A brief summary of the electron-phonon scattering is discussed in Section III. In this section, we will review the latest theoretical developments aimed at exploring the effect of electron-phonon interactions on carrier mobility. In the last section, we will describe the simulation approach we use. In this section, we also present the simulation results to discuss the acoustic phonon scattering effect on the charge carrier mobility.

2. Electronic strcutures of CNTs

2.1. Structure of CNTs

The SWCNT is a hollow cylinder-shaped molecule with a diameter in the order of 1 nm. SWCNT can be viewed conceptually as graphene sheets rolled up into concentric cylinders. The atomic structure of a single-walled CNT is conveniently explained in terms of two vectors C_h and T. T is called translational vector, it defines the direction of CNT axis. C_h is called chiral vector, representing the circumference of a CNT. A specific SWCNT is defined by two integers (n,m) with $n \geq m \geq 0$ related to the chiral vector $C_h = n\mathrm{a}_1 + m\mathrm{a}_2$, where a_1 and a_2 are the basis vectors ofthe graphene lattice as shown in Fig.1a. Fig.1b shows the chiral vector for a so-called (5,5) armchair nanotube, where the SWCNT is made by joining the ends of the chiral vector, *i.e.*, dashed blue lines. Three categories of SWCNT are now defined: the armchair (n,n), the zigzag (n, 0) and the chiral nanotube (n, m) with n > m > 0 (see Figure Fig.1b, Fig.1c, Fig.1d).

2.2. Electronic structure of CNTs

The electronic structure of a SWCNT is deduced from the energy dispersion of graphene. The band structure of the SWCNT is found by imposing periodic boundary conditions around the circumference of the tube, *i.e.*, the wave function has to be single valued:

$$\Psi_k(r + C_h) = \Psi_k(r) \tag{1}$$

where k is a wave vector and r is a real space lattice vector of the graphene lattice. This leads to periodic boundary condition in momentum space

http://dx.doi.org/10.5772/51451

$$k \cdot C_h = 2\pi p \tag{2}$$

Where p is an integer. In other words, the k-vector projected onto the chiral vector $k_{//}$ (along the circumference) becomes quantized, while the k-vector $k\perp$ along the tube axis is continuous for an infinite nanotube. The 1D dispersion or band structure of a SWCNT is thus made of the energy bands related to different quantized values p as a function of $k\perp$. Whether or not these quantization lines cross a K-point makes the SWCNT a metal or a semiconductor.

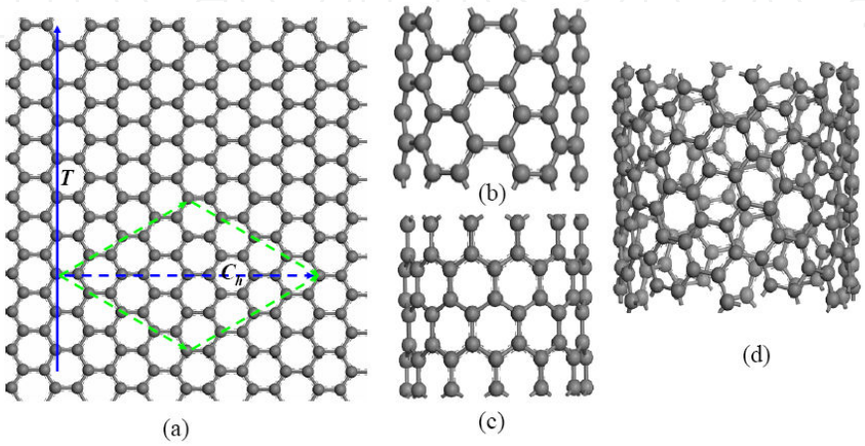

Figure 1. a) The example of folding a (4,4) armchair SWCNT from the graphene sheet. C_h and T are the chiral and the translation vectors of the SWCNT, respectively. (b), (c), and (d) are the structure of different kinds of SWCNTs. (b) A (6, 6) armchair SWCNT. (c) A (12, 0) zigzag SWCNT. (c) A chiral (12, 6) SWCNT.

For the armchair SWCNTs, these nanotubes are truly metallic and have two bands crossing at the Fermi level (Figure 2a). The bands stem from the quantization lines drawn in Figure 2d in the reciprocal lattice. The corners of the hexagons are the K-points, where the conduction and the valence band of the graphene dispersion touch. One of the quantization lines (thick dashed line) passes through two K-points making the tube metallic.

Figure 2b shows the band structure for a (15, 0) zigzag tube which is metallic judging from the degenerate band crossing the Fermi level. The bands stem from the quantization lines drawn in Figure 2e. It is seen that the bands touching at the Fermi level are two times degenerate. However, the band structure is calculated from the dispersion graphene, while the CNT has a curvature around the circumference of the tube. The curvature slightly modifies the band structure by moving the K-points.For the zigzag tube with n ≠ 3*integer, such as (16, 0) zigzag tube (Figure 2c), in the reciprocal space the quantization lines do not cross the K-points. It has a band gap in the order of ~ 1eV.

So, theoretical studies have shown that a single-walled CNT can be either metallic or semiconducting depending on its chirality and diameter. The armchair SWCNTs are a group of truly metallic conductors with two bands crossing the Fermi level. For n-m=3*integer, the nanotubes would be quasi-semiconducting with a small band gap proportional to $1/d^2$. Typical band gaps are in the order of tens of meV. Finally, a group of zigzag and chiral SWCNTs

is semiconducting (n-m ≠ 3*integer) with bigger band gaps. The band gap of these tubes are in the order of ~1 eV and scales as $E_{gap} \sim 1/d$, where d is the diameter of the SWCNT [36].

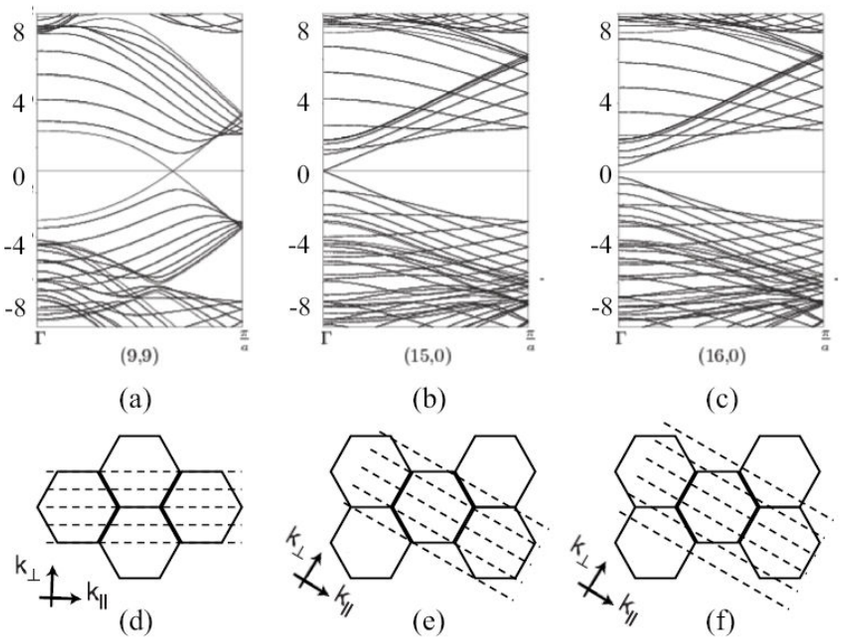

Figure 2. a) The band structure of a (9,9) armchair nanotube. One of the quantization lines bands crossing the Fermi energy stem from the quantization line in (d), which crosses the K-points and makes this SWCNT metallic. (b) The band structure of a (15,0) zigzag nanotube. It has a doubly degenerate band crossing the Fermi level in (e). When the curvature effects are taken into account the K-points move from the corners of the hexagon to the red dots, which makes metallic zigzag nanotubes to be small band gap semiconductors. (c) and (f) Some tubes are semiconducting with a bigger band gap as the (16,0) zigzag tube.

2.3. Electronic transport of CNTs

For the metallic armchair CNTs, the valence and conduction bands cross at the Fermi level just as in the case of graphene. The two crossing bands provide the tube with two conducting channels at and close to the Fermi level, where in each of these bands, two electrons of opposite spins can co-exists. By the Landauer formula, the conductance is then:

$$G = (4e^2/h)T \tag{3}$$

where e is the electron charge, h is Planck's constant, and T is the transmission coefficient for electrons through the sample. The conductance of a ballistic SWCNT with perfect contacts (T = 1) is then: $R_{CNT} = 4e^2/h \approx 150\ \mu S$, corresponding to a resistance of 6.5 kΩ. In addition, the scattering of charge carriers along the length of CNTs results in a Drude-like resistance. The presence of scatterers that gives a mean free path l for backscattering contributes an ohmic resistance to the tube, $R_d \propto L/l$, where L is the length of CNT. Thus, the total resistance of a SWCNT contacted by metal leads on both ends is sum of these two contributions: $R_{tot} = R_{CNT} + R_d$.

http://dx.doi.org/10.5772/51451

Different band structures are obtained for a truly metallic, a quasi-metallic and a semiconducting nanotube. The various band structures are illustrated in Figure 2 which displays a quasi-metallic (15,0) zigzag, a semiconducting (16,0) zig-zag, and an armchair (9,9) SWCNT band structure. In the case of the armchair tube, the two bands conduct the current while in the case of quasi-metallic zigzag or chiral SWCNTs, a small energy gap of few meV exists due to the nanotube curvature. This gap is important at low-temperatures and can suppress electron transport. However, at room-temperature, the thermal energy is larger than the gap and the tubes show metallic behavior. Semiconducting tubes possess an energy-gap of ≈ 0.5-1 eV, where zigzag SWCNTs have their DOS singularities at the Γ-point.

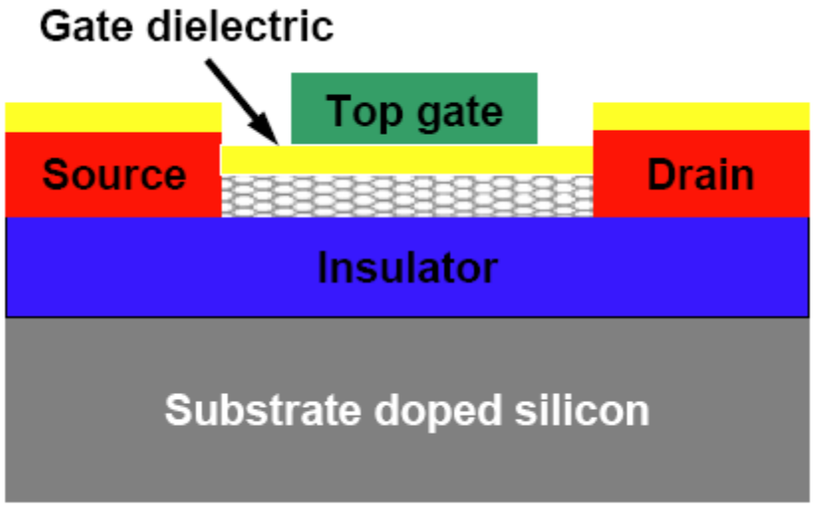

Figure 3. The model of planar-structure CNTFET

CNT filed effect transistor (CNTFET) can distinguish between the two character types. In the case of metallic tubes, the conductance is V_G independent, with the crossing bands providing conducting electrons independently on the V_G, i.e., the gate potential does not change the number of conduction channels. On the other hand, the conductance in semiconducting tubes is strongly affected by the V_G and can change by orders of magnitude. The CNT has an atomic and electronic structure that gives it unique advantage as an FET channel.

3. Electron-phonon scattering in CNTs

CNTs have been extensively explored for nanoelectronic applications due to their excellent electrical properties. Scattering plays an important role on carrier transport CNTs [13, 14]. It has demonstrated that at finite temperatures or high biases, electron-phonon scattering becomes significant. It can be divided into the low- and high-energy regimes, corresponding to acoustic-phonon scattering and optical- or zone-boundary-phonon scattering. Because of the light mass and strong bonds, the optical-phonon energy is very high in CNTs

$\hbar\omega_0 \sim 160meV\, k_B T$ at 300 K, meaning that these phonons are not thermally populated, which is one of the reasons for the high room-temperature mobilities in CNTs.At small source-drain biases and moderate temperatures the mean free path in clean tubes is set by acoustic-phonon scattering, as shown by a number of experimental and theoretical works (15, 37, 38). A straightforward calculation shows that, when the Fermi level is in the linear part of the electron dispersion relation, the scattering rate for a tube of linear mass density ρ and sound velocity v_s is given by:

$$\frac{1}{\tau_{ac}} \cong \frac{\pi}{\hbar}(d E_g \Big/ d\varepsilon)\frac{k_B T}{\rho v_s^2}\frac{1}{h\, v_F} \tag{4}$$

The coupling is through the strain dependence of the band gap. Depending on the tube, the dominant coupling can either be through the stretching or the twisting of the tube. The linear temperature dependence comes from the thermal occupation of the (small-momentum transfer) acoustic phonon responsible for backscattering.In addition to the low-energy acoustic phonons, electron (or hole) scattering by the radial breathing mode (RBM) is important in the low bias regime. The RBM phonon energy is inversely proportional to the tube diameter8, and its energy is comparable to the thermal energy at room temperature for tubes in the diameter range of d_{CNT} = 1.5–2.0 nm, which are of interest for electronic applications. As the acoustic mean free path is very long-of the order of a micrometre at room temperature-electrons can be accelerated up to the RBM energy not only thermally, but also by an applied bias of a few Vcm^{-1}

Unlike acoustic phonon scattering, optical phonon scattering is very strong in CNTs; optical phonons contract and elongate the C–C bond length and lead to a strong modulation of the electronic structure. However, for electrons to emit an optical phonon, their energies must be larger than the optical phonon energy. This can only be achieved under high bias conditions. Such scattering processes were first observed in metallic tubes [13, 14, 15] and later in semiconducting tubes [39]. At large source-drain biases, the electrons in the tube can accelerate to energies well above the Fermi energy, and these hot electrons can scatter very efficiently by emitting optical and zone-boundary phonons. The scattering rate for this process is

$$\frac{1}{\tau_q^{\alpha}} \cong \frac{2\pi}{\hbar} \mid D_{k,q}^{\alpha} \mid^2 \frac{2\hbar}{\rho\Omega_q^{\alpha}}\frac{1}{h\, v_F}\left(\langle n\rangle + \frac{1}{2}\right) \tag{5}$$

Where $D_{k,q}^{\alpha}$ is the matrix element, Ω_q^{α} is the phonon frequency, and <*n*> is the occupancy of the mode in the branch α with wave vector q. This process is rapid, resulting in mean free paths that are measured to be in the range of 10 nm [13, 14], a hundred times shorter than the micro-scale mean free paths at small biases.

In summary, the inelastic scattering rates determining transport properties of CNTs vary by four orders of magnitude depending on the energy of the electrons and their angular momentum (sub-band index) as shown in Figure 4 [40]. The weakest is the acoustic (primarily

http://dx.doi.org/10.5772/51451

RBM) phonon scattering, which has linear temperature dependence. The optical phonon scattering rate, which is two orders of magnitude stronger, is nearly temperature independent. Finally, another two orders of magnitude stronger than the optical phonon scattering is impact excitation.

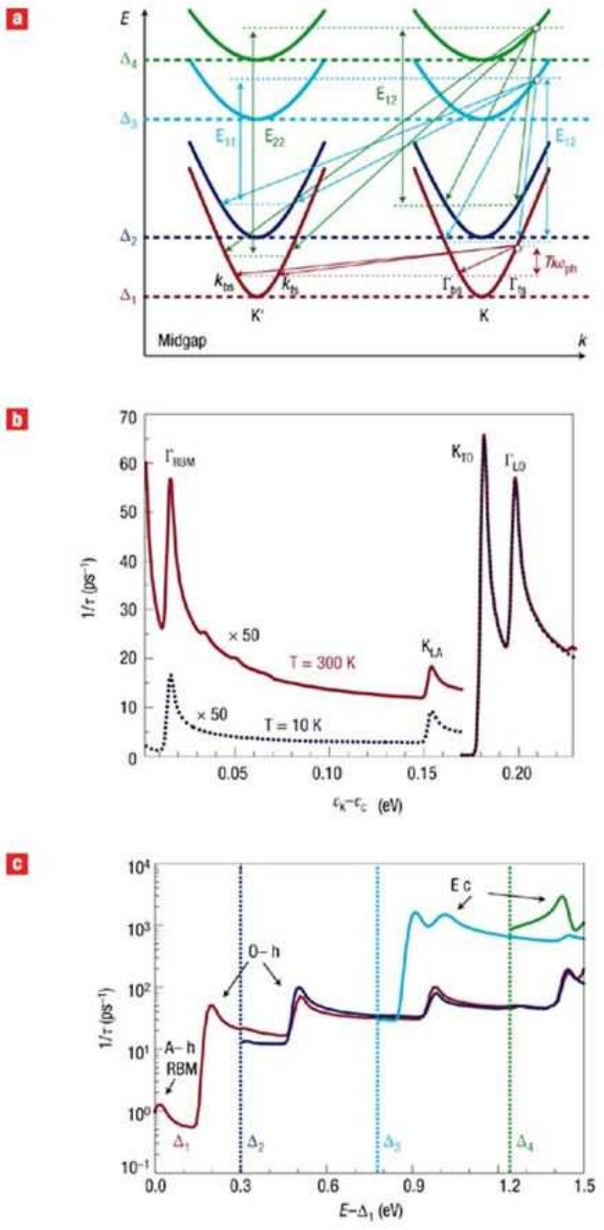

Figure 4. a), Schematic illustration of the intra-sub-band (*Γ*) and inter-sub-band (K) phonon scattering mechanisms (red) and electron impact excitation (blue and green curves) for the first four conduction bands.

The different conduction band edges are labelled as Δ_i and the resulting electronic excitations are denoted as E_{iij}. Subscripts bs and fs stand for the back and forward scattering. b), Calculated phonon scattering rate for a (25,0) nanotube showing weak acoustic phonon scat-

tering and strong optical phonon scattering. c), Calculated inelastic scattering rate for a (19,0) nanotube over a wide carrier energy range. Different colours correspond to the scattering rates of electrons in bands with different circumferential angular momentum. The vertical lines show the bottoms of the conduction bands 2 (blue), 3 (cyan) and 4 (green) with respect to the fundamental band edge Δ_1. Some of the characteristic peaks in the scattering, due to the longtitudinal (LA) acoustic phonons (A-Ph), radial breathing mode (RBM), longitudinal (LO) and transverse (TO) optical phonons (O-Ph) and impact electronic excitation (I-Exc), are labelled. In b and c the electron scattering rate is shown as a function of the excess energy of the electron above the first conduction-band minimum. (Figure 2 in ref. 40)

4. Acoustic phonons scattering effect on carrier mobility of semiconducting SWCNTs

A number of groups have reported modeling and simulation studies of the carrier transport in CNTs [41-48]. Our intent in this section is not to review these works. Instead, we briefly describe the techniques we currently use to study the intrinsic carrier mobility of semiconducting SWCNTs. The semiconducting zigzag SWCNTs have large intrinsic carrier mobility due to the weak acoustic phonon scattering. Although recently much experimental progress has been achieved on improving the charge carrier mobility of semiconducting CNTs [8, 11, 49, 50], there are a lot of works on the theoretical understanding of the carrier mobility in the semiconducting zigzag SWCNTs [16, 18, 22, 51]. The carrier mobility of the semiconducting zigzag SWCNT can reach 7.9×10^4 cm^2/Vs at room temperature experimentally [8]. Even the higher mobility up to 1.2×10^5 cm^2/Vs for a 4.6 nm diameter semiconducting zigzag SWCNT at room temperature has been predicted by the zone-folding method approximation [16]. Perebeinos *et. al.* [18] studied the electron-phonon scattering in the semiconducting zigzag SWCNTs by using the tight-binding model. They found that under high fields, the dominant scattering mechanism is interband scattering by the longitudinal optical phonons, while under very low field, the scattering is entirely from the acoustic phonons. The acoustic phonon scattering process could be appropriately described by using the deformation-potential theory [52-55], which has been used extensively in carbon nanostructures and the tightly packed organic molecular crystals.

4.1. Acoustic phonons scattering based on the deformation-potential theory

The spedific conducitivity of a three-dimensional solid can be written as:

$$\sigma = q(n_e\mu_e + n_h\mu_h) \tag{6}$$

where n_e and n_h are the density of mobile electrons and holes, respectively, and μ_e and μ_h are their mobilities, respectively.

http://dx.doi.org/10.5772/51451

Bardeen and Shockley [52] derived an analytical expression for the intrinsic carrier mobility (μ) by assuming that the change of the energy of the electron scattered by an acoustic phonon is proportional to the deformation:

$$\mu_e = \frac{2^{3/2}\pi^{1/2}}{3} \frac{c_\perp \hbar^4 e}{\varepsilon_{1e}^2 m_e^{*5/2} (k_B T)^{3/2}} \tag{7}$$

$$\mu_h = \frac{2^{3/2}\pi^{1/2}}{3} \frac{c_\perp \hbar^4 e}{\varepsilon_{1h}^2 m_h^{*5/2} (k_B T)^{3/2}} \tag{8}$$

Here $\varepsilon_{1e}$and ε_{1h} are the deformation potentials, defined as:

$$\varepsilon_{1e} = \frac{\delta W_{c,l}}{\Delta},\ \varepsilon_{1h} = \frac{\delta W_{v,u}}{\Delta} \tag{9}$$

Beleznay *et. al.* [53] reformulated the analytical expression of the carrier mobility in the one dimensional case to study the charge transport in the guanine stack. During the propagation of acoustic wave, the stretching vibration of the crystal lattices may be expressed as:

$$\delta\vec{r} = A_q \hat{I}_q \cos(\vec{q} \bullet \vec{r} - \omega_q t) = \frac{1}{2} A_q \hat{I}_q [e^{i(\vec{q}\bullet\vec{r}-\omega_q t)} - e^{-i(\vec{q}\bullet\vec{r}-\omega_q t)}] \tag{10}$$

where A_q is amplitude, $\vec{q}$ is wave vector, is the unit vector along the direction of propagation, $\hat{I}_q$ is the angular frequency of vibration. The displacement difference between two points with mean distance a (a is the lattice constant in one dimension):

$$\delta\vec{r}(a) - \delta\vec{r}(0) = a(\nabla_r \delta\vec{r}) \tag{11}$$

The deformation potential theory proposed by Bardeen and Schockly is based on the face that when the change of lattice is very small, the variations of the top of valance band and the bottom of conduction band are linearly related to the variation of lattice constant, therefore the energy of the top of valence band (E_v) and the energy of the bottom of conduction band (E_c) may be expressed as follows:

$$E_v = E_{0v} + E_{1v}\Delta(\vec{r});\ E_c = E_{0c} + E_{1c}\Delta(\vec{r}) \tag{12}$$

Where $\Delta=\delta a/a$, E_{0c} and E_{0v} are the energies to the top of valence band and bottom of conduction band, respectively, in the undeformed crystal. Bardeen and Schockly proved that $E_1\Delta(\vec{r})$ may be considered as preturbational potential and referred to the following expression:

$$\delta U(\vec{r}) = E_1 \Delta(\vec{r}) = E_1(\nabla_r \delta\vec{r}) \tag{13}$$

The matrix element obtained form perturbational potential is $H_{k'k} = \psi_{k'} \mid \delta U \mid \psi_k = E_1 \psi_{k'} \mid \nabla_r \delta\vec{r} \mid \psi_k$ We consider only the 1st Brillouin zone by expanding $u_k(\vec{r})$ and neglecting the terms of higher order and then integrate with respect to the unit cell to derive

$$\left| H_{k'k} \right|^2 = \frac{1}{4} q^2 A_q^2 E_1^2,\ k - k' \pm q = 0 \tag{14}$$

Upon considering the crystal as continuous medium, time-averaging and summing for the whole crystal, one can get the total average kinetic energy for the whole crystal :

$$E_T = \frac{1}{2} \rho L\ A_q^2 \omega_q^2 \tag{15}$$

When the temperatures is higher than Debye temperature, based on classical law of equipartition energy, we have

$$E_T = \frac{1}{2} \rho L\ A_q^2 \omega_q^2 = \frac{1}{2} k_B T \tag{16}$$

Where $\omega_q = C_l q$, C_l is the velocity of longitudinal wave. Thus, we obtain

$$\left| H_{k'k} \right|^2 = \frac{1}{4} q^2 A_q^2 E_1^2 = k_B T E_1^2 \Big/ 2\rho L\ C_1^2 \tag{17}$$

From quantum mechanical theory, the scattering probability from $\vec{k}$ to $\vec{k}'$ is:

$$\Theta(k', k) = \frac{2\pi}{\hbar} \left| H_{k'k} \right|^2 \delta[E(k) - E(k') \pm \hbar\omega_q] \tag{18}$$

For the very small energy of phonon the scattering may be considered as elastic, and by summing up the probabilities of phonon absorption and emission. From quantum theory of solid, the reciprocal of relaxation time is:

$$\frac{1}{\tau} = \sum_{k'} \Theta(k', k)(1 - k_z / k_z') \tag{19}$$

With the effective mass approximation, we can get:

$$\frac{1}{\tau}=\frac{2(2m^*)^{1/2}k_BTE_1^2}{\hbar^2\rho C_1^2}(E-E_0)^{-1/2} \tag{20}$$

In semiconductor physics the mobility is defined by

$$\mu=e\tau/m^* \tag{21}$$

By using Boltzmann distribution function, we can get the charge mobility in one dimensional crystal:

$$\mu=\frac{e\bar{\tau}}{m^*}=\frac{e\hbar^2C}{(2\pi k_BT)^{1/2}m^{*3/2}E_1^2} \tag{22}$$

where $\bar{\tau}$ is the average scattering relaxation time of the acoustic phonon, m^* is the effective mass of the charge, C is the stretching modulus, E_1 is the deformation-potential constant. $\bar{\tau}$, m^* and C are defined as:

$$\bar{\tau}=\hbar^2C/\left(2\pi m^*k_BT\right)^{1/2}E_1^2 \tag{23}$$

$$m^*=\hbar^2[\partial^2E(k)/\partial k^2]^{-1}\big|_{k=0} \tag{24}$$

$$C=a_0[\partial^2E(k_F)/\partial a^2]\big|_{a=a_0} \tag{25}$$

$$E_1=\delta E(k_F)a/\delta a \tag{26}$$

where $E(k)$ is the energy band and a is the lattice constant, the deformation-potential constant $E_1=\delta E(k_F)a/\delta a$, where $\delta E(k_F)$ is the conduction or valence band shift near Fermi surface that caused by the small change δa in the lattice constant. Although all of these quantities in Eq (23) are obtained from the first-principles calculations, it is a simple view of the full Boltzmann transport equation, and this method have been previously applied in the study of the graphene nanoribbons [54] and the functionalized CNTs [55].In this simple approximation, we could find that the intrinsic carrier mobility scattered by the longitudinal acoustic phonons varies with the temperature approximately as $T^{-1/2}$, not the empirical relation T^{-1} by the experimental captured, which is the combined result of other scattering mechanisms.

4.2. Calculation method and results

To calculate the carrier mobility of the semiconducting zigzag SWCNTs, there are three parameters to be determined as shown in the above formula, namely, m^*, C, and E_1. All these

parameters can be calculated by the first-principles method. The density functional theory calculations were performed with *Vienna ab initio simulation pack* (VASP) code [56, 57], using Perdew-Burke-Ernzerhof exchange-correlation functional [58]. In the first principles calculations, the ion-electron interactions were treated with the projected augmented wave (PAW) approximation [59, 60]. The plane wave cutoff energy was set to 500 eV and the convergence threshold for energy was 10^{-5} eV. Brillouin Zone integration was carried out at 1×1×25 Monchorst-Pack k-grids, and 150 uniform k-points along the one-dimensional Brillouin Zone are used to obtain the band structures. The symmetric unrestricted optimizations for geometry are performed using the conjugate gradient scheme until the force acting on every atom is less than 10 meV/Å. To obtain the value of the stretching modulus C and the deformation-potential constant E_1, we calculated the band structures of unit cells under the uniaxial stress applied along the periodic direction, allowing a unitary deformation in the range of ±0.01%. With the changes of the energy at Fermi energy two straight lines with the correlation coefficient >0.999 are obtained. From the slope of the straight lines, the deformation-potential constants E_1 are obtained. The stretching modulus C can be estimated from the variance obtained from the second derivative of the total energy upon unitary deformation.

Electronically, SWCNTs can behave as either metallic or semiconducting depending on the chirality of their atomic arrangements and diameter. The band structure calculations have predicted that the armchair SWCNTs with (n, n) indices are truly metallic with the finite density of states at Fermi level, whereas the zigzag SWCNTs are metallic, if n is a multiple of 3 and all others are semiconducting in the unstrained condition. So the semiconducting zigzag SWCNTs with (n, 0) indices selected for the simulation correspond to $n=3q+1$ *and* $3q+2$ (q= 2, 3, 4, 5, and 6) in this paper.

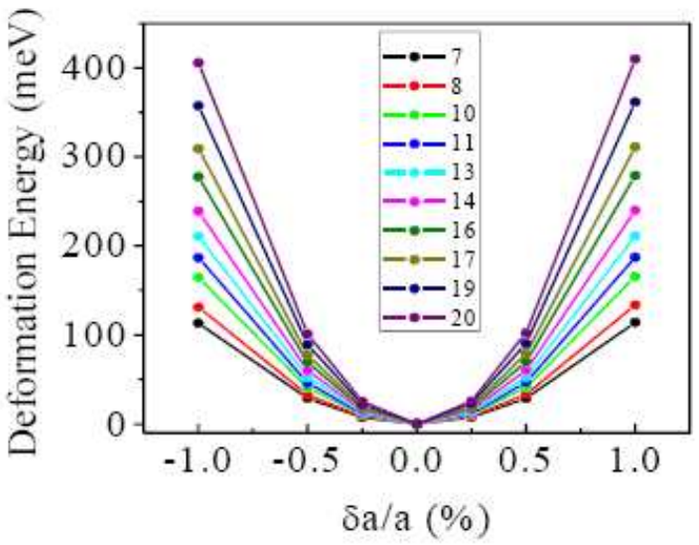

Figure 5. Deformation energy as a function of compressing and elongating the semiconducting zigzag SWCNTs along the longitudinal direction.

http://dx.doi.org/10.5772/51451

The stretching modulus was evaluated by compressing and elongating the semiconducting zigzag SWCNTs along the longitudinal direction. For the evaluation of the elastic properties all atomic positions were fully relaxed. Typically the unstrained configurations were calculated first and then the strain was applied in steps of 0.25% in units of strain percentage for strains less than 1%. The results of these simulations are presented in Figure 5. It clearly demonstrates the parabolic form of the strain energy as a function of the strain, reminiscent to the parabolic potential energy derived from Hook's law for the macroscopic springs. It is interesting to note that the same strain can lead to the increasingly high deformation energies in SWCNT with larger n, due to the additivity of the energy required to compress/elongate a larger number of carbon-carbon bonds, within the SWCNT network. The second derivative of the total energy could be obtained easily. The stretching modulus was also shown in Figure 6.

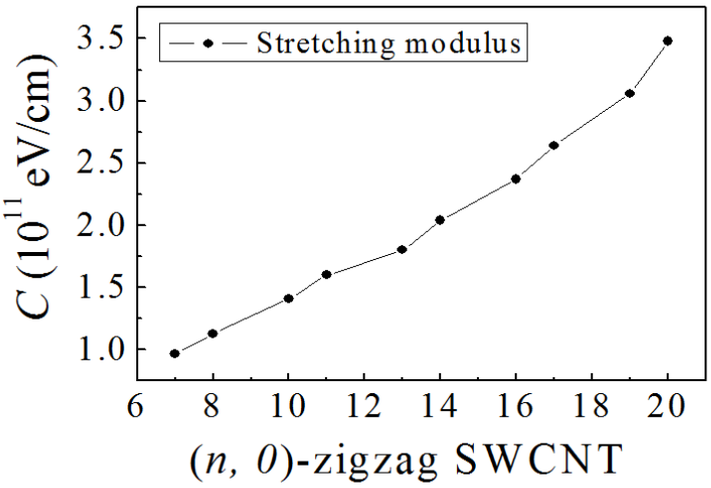

Figure 6. The calculated stretching modulus C of semiconducting zigzag SWCNTs as a function of n.

From the shape of the band structure, we have calculated the effective masses of the electrons and holes of the semiconducting zigzag SWCNTs. We can fit two curves the energy $E(k)$ versus k points for the bottom of the conduction band and the top of the valence band near Γ point, so we got the effective mass m_e^* and m_h^* for electron and hole, respectively, as shown in Figure 7. We can see that the effective masses of holes of SWCNTs are smaller than those of electrons for $n=3q+1$, while it is just opposite for $n=3q+2$. This is due to the curvature effects. The obtained effective masses of the semiconducting zigzag SWCNTs, are quite well in agreement with the earlier theoretical reported values [61].

The deformation-potential constant E_1, which represents the scattering of an electron or hole from the acoustic phonon, was calculated from the algebraic average of the band edge shifts in the cases of the dilatation and compression. E_c and E_v are the deformation-potential constants for the conduction band and the valence band, respectively. The deformation-potential constants, E_c and E_v, calculated from the band edge shifts of the bottom of the

conduction band and the top of the valence band as shown in Figure 8b and Figure 4c. The deformation-potential constants, E_c and E_v, as a function of the deformation proportion for q=2, 3, 4, 5, and 6 are displayed in Figure 8a. It is noted that E_c is larger than E_v in one order of magnitude for $n=3q+2$; while E_c is less than E_v in one order of magnitude for $n=3q+1$. Except for n=8, we find that there is always one of the deformation-potential constants about 14 eV between E_c or E_v. This is agreement with the previous result.[12]

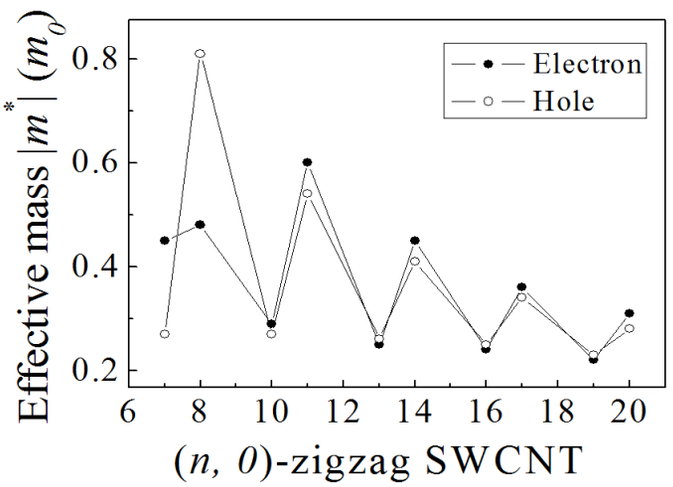

Figure 7. The electron and hole effective masses $|m^*|$ of semiconducting zigzag SWCNTs as a function of n.

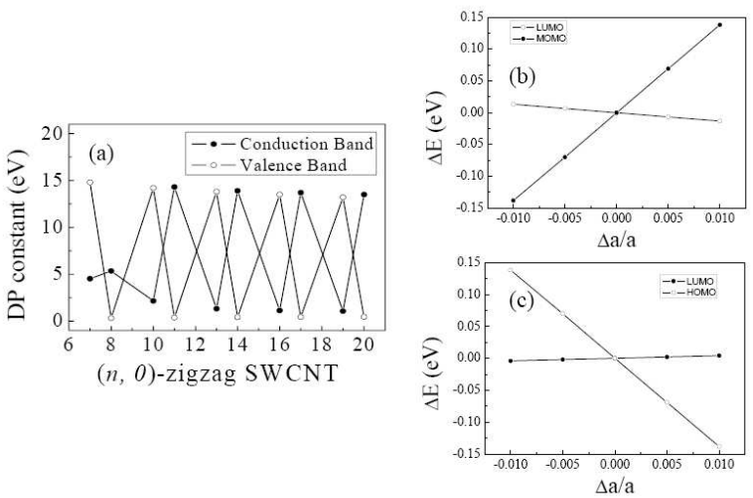

Figure 8. a): The deformation-potential (DP) constants E_c and E_v of semiconducting zigzag SWCNTs as a function of n. b) and c): Band edge shifts of the bottom of conduction band and the top of valence band as a function of deformation proportion for (13, 0) and (14, 0) SWCNT, respectively.

The calculated effective masses, the stretching modulus, and the deformation-potential constants of the semiconducting zigzag SWCNTs are summarized in Table 1. The electron and

http://dx.doi.org/10.5772/51451

hole mobilities at room temperature can be calculated by the Eq (23) from these three parameters are also displayed in Table 1. We plotted the mobilities of electrons and holes of the semiconducting zigzag SWCNTs calculated as a function of the diameter in Figure 9.

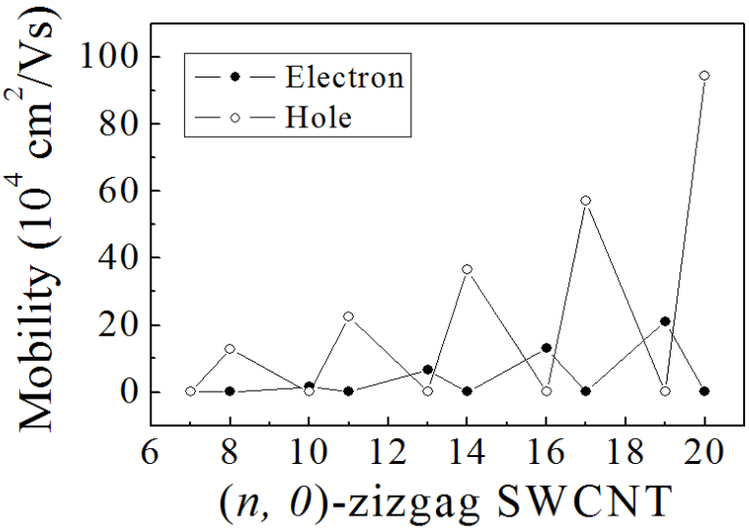

Figure 9. The mobilities of electron μ_e and hole μ_h of the semiconducting zigzag SWCNTs as a function of n.

n	*7*	*8*	*10*	*11*	*13*	*14*	*16*	*17*	*19*	*20*
$M_e^*(m_0)$	0.45	0.48	0.29	0.60	0.25	0.45	0.24	0.36	0.22	0.31
$M_h^*(m_0)$	0.27	0.81	0.27	0.54	0.26	0.41	0.25	0.34	0.23	0.28
$C(10^{11}$eV/cm)	0.97	1.13	1.41	1.60	1.80	2.04	2.37	2.64	3.06	3.48
E_c(eV)	4.52	5.35	2.15	14.3	1.32	13.9	1.12	13.7	1.06	13.5
E_v(eV)	14.8	0.31	14.2	0.37	13.8	0.41	13.5	0.43	13.2	0.44
$\mu_e(10^3$cm^2/Vs)	1.31	0.92	15.5	0.14	65.6	0.28	130	0.52	209	0.88
$\mu_h(10^3$cm^2/Vs)	0.25	128	0.41	224	0.56	367	0.89	571	1.24	945

Table 1. The calculated effective masses $|m^*|$

(m_e^*, m_h^*), the stretching modulus C, the deformation constants E_c and E_v, and the mobilities of electron μ_e and hole μ_h for the semiconducting zigzag SWCNTs for n = 7, 8, 10, 11, 13, 14, 16, 17, 19, and 20.

It is found that the intrinsic electron mobility can reach 2×10^5 cm^2/Vs at room temperature for *n=19*, and the hole mobility is calculated as 10^6 cm^2/Vs at room temperature for *n=20*. We find that the mobility exhibits a distinct alternating behavior: for *n=3q+1*, the intrinsic hole room-temperature mobility is about in two orders of magnitude less than that of electron;

for $n=3q+2$, the intrinsic hole room-temperature mobility is about in two orders of magnitude larger than that of electron. It is in consistent with DP constant, E_c or E_v, which is related to the band-edge shift induced by the scattering of an electron (conduction band edge) or hole (valence band edge) from the acoustic phonon.

To understand the alternating behavior of DP constant, we examine the frontier molecular orbitals at the Γ-point, i.e., the highest occupied molecular orbital (HOMO) for the hole and the lowest unoccupied molecular orbital (LUMO) for electron, see Figure 10, For n = 7, it is found that the bonding direction of HOMO is perpendicular to the longitudinal direction and it is of anti-bonding character along the transport direction. While for the LUMO, the bonding direction is along the stretching direction. The bonding state is stable and anti-bonding state is unstable, which means the site energy of anti-bonding state is more prone to change when the structure is deformed. The band-edge shift due to CNT stretching comes from the site energy change. Thus, DP constant of hole state (HOMO) is larger than that of electron state (LUMO), and hole is scattered more strongly by acoustic phonons than electron. However, for n = 8, the LUMO is vertically to the longitudinal direction, while the HOMO is along the longitudinal direction.

It is thus expected that for $n=3q+1$, the hole state (HOMO) is scattered much more strongly than the electron state (LUMO) from the acoustic phonon, while it is just opposite for $n=3q+2$. So the alternating behaviors of the carrier mobilities of the semiconducting zigzag SWCNT are reasonable.

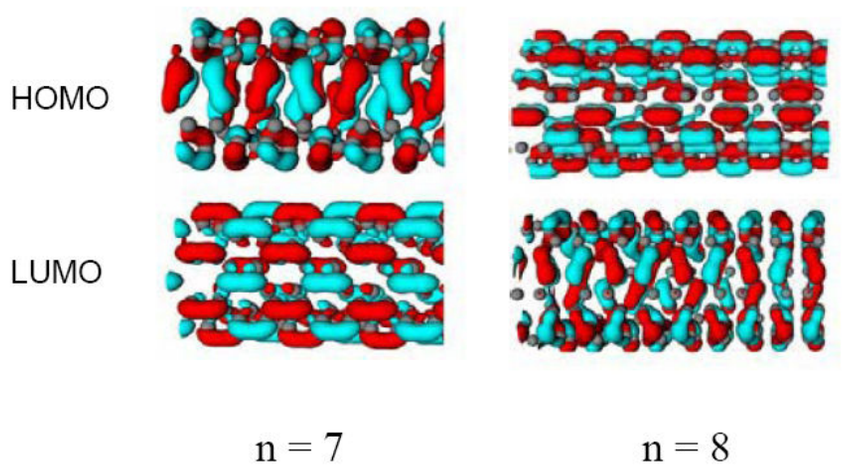

Figure 10. The Γ-point HOMO and LUMO wave functions for the zigzag SWCNT with n = 7 and n = 8.

5. Conclusion

CNTFETs are important devices with potentially important applications in nanoelectronics. In this work, we have summarized the electron-phonon scattering on the carrier transport.

http://dx.doi.org/10.5772/51451

The carrier mobility of the semiconducting zigzag SWCNT scattered from the acoustic phonons is investigated by using first-principles calculations. We considered only the longitudinal acoustic phonon scattering process by using the deformation-potential theory. We found that the intrinsic carrier mobility can reach 10^6 cm^2/Vs at room temperature for n=20, and the intriguing alternating behaviors of the carrier mobilities of the semiconducting zigzag SWCNTs are due to the curvature effects of the CNT. We believe that the detailed investigation of acoustic phonon scattering in CNTs [62] will also help us to study the carrier mobilities in other organic or inorganic materials by using the similar technique.

Acknowledgements

This work is supported by the Fundamental Research Funds for the Central Universities, a Project Funded by the Priority Academic Program Development of Jiangsu Higher Education Institutions (PAPD). Bo Xu thanks the support by the China Postdoctoral Science Foundation funded project (20100481119) and Jiangsu Planned Projects for Postdoctoral Research Funds (1002007B).

Author details

Bo Xu[1], Jiang Yin[1] and Zhiguo Liu[1]

1 Department of Materials Science and Engineering, Nanjing University, People's Republic of China

References

[1] Iijima, S. (1991). Helical Microtubules of Graphitic Carbon. *Nature*, 354, 56-58.

[2] Bachtold, P.H., Nakanishi, T., & Dekker, C. (2001). Logic Circuits with Carbon Nanotube Transistors. *Science*, 294, 1317-1320.

[3] Tans, S. J., Verschueren, A. R. M., & Dekker, C. (1998). Room-temperature transistor based on a single carbon nanotube. *Nature*, 393, 49-52.

[4] Radosavljevic, M., Freitag, M., Thadani, K. V., & Johnson, A. T. (2002). Nonvolatile molecular memory elements based on ambipolar nanotube field effect transistors. *Nano Lett.*, 2, 761-764.

[5] Kong, J., Franklin, N. R., Zhou, C., Chapline, M. G., Peng, S., Cho, K., & Dai, H. (2000). Nanotube Molecular Wires as Chemical Sensors. *Science*, 287, 622-625.

[6] Frank, S., Poncharal, P., Wang, Z. L., & de Heer, W. A. (1998). Carbon nanotube quantum resistor. *Science*, 280, 1744-1746.

[7] Kong, J., Yenilmez, E., Tombler, T. W., Kim, W., & Dai, H. (2001). Quantum interference and ballistic transmission in nanotube electron waveguide. *Phys. Rev. Lett*, 87, 106801.

[8] Javey, J.G., Wang, Q., Lundstrom, M., & Dai, H. J. (2003). Ballistic carbon nanotube field-effect transistors. *Nature*, 424, 654-657.

[9] Javey, J.G., Farmer, D. B., Wang, Q., Yenilmez, E., Gordon, R. G., Lundstrom, M., & Dai, H. J. (2004). Self-aligned ballistic molecular transistor and electrically parallel nanotube arrays. *Nano Lett.*, 4, 1319-1322.

[10] Lin, Y. M., Appenzeller, J., Chen, Z., Cgen, Z. G., Cheng, H. M., & Avouris, P. H. (2005). High-performance dual-gate carbon nanotube FETs with 40nm gate length. *IEEE Electron Device Lett.*, 26, 823-825.

[11] Durkop, T., Getty, S. A., Cobas, E., & Fuhrer, M. S. (2004). Extraordinary mobility in semiconducting carbon nanotubes. *Nano Lett.*, 4, 35-39.

[12] Zhou, X., Park, J. Y., Huang, S., Liu, J., & Mc Euen, P. L. (2005). Band structure, phonon scattering, and the performance limit of single-walled carbon nanotube transistors. *Phys. Rev. Lett.*, 95, 146805.

[13] Yao, Z., Kane, C. L., & Dekker, C. (2000). High-field electrical transport in single-wall carbon nanotubes. *Phys. Rev. Lett.*, 84, 2941.

[14] Javey Guo, J., Paulsson, Q., Wang, D., Mann, M., & Lundstrom, H.D. (2004). High-field quasiballistic transport in short carbon nanotubes. *Phys. Rev. Lett.*, 92, 106804.

[15] Park, J. Y., Rosenblatt, S., Yaish, Y., Sazonova, V., Üstünel, H., Braig, S., Arias, T. A., Piet, W., Brouwer, Paul. , & Mc Euen, L. (2004). Electron-phonon scattering in metallic single-walled carbon nanotubes. *Nano Lett.*, 4, 517-520.

[16] Pennington, G., & Goldsman, N. (2003). Semiclassical transport and phonon scattering of electrons in semiconducting carbon nanotubes. *Phys. Rev. B.*, 68, 045426.

[17] Pennington, G., & Goldsman, N. (2005). Low-field semiclassical carrier transport in semiconducting carbon nanotubes. *Phys. Rev. B*, 71, 205318.

[18] Perebeinos, V., Tersoff, J., & Avouris, P. H. (2005). Electron-phonon interaction and transport in semiconducting carbon nanotubes. *Phys. Rev. Lett.*, 94, 086802.

[19] Perebeinos, V., Tersoff, J., & Avouris, P. H. (2006). Mobility in semiconducting carbon nanotubes at finite carrier density. *Nano Lett.*, 6, 205-208.

[20] Verma, M. Z., Kauser, Z., & Ruden, P.P. (2005). Ensemble Monte Carlo transport simulations for semiconducting carbon nanotubes. *J. Appl. Phys.*, 97, 114319.

[21] Verma, M. Z., Kauser, , & Ruden, P. P. (2005). Effects of radial breathing mode phonons on charge transport in semiconducting zigzag carbon nanotubes. *Appl. Phys. Lett.*, 87, 123101.

[22] d'Honincthun, H. C., Retailleau Galdin, S., See, J., & Dollfus, P. (2005). Electron-phonon scattering and ballistic behavior in semiconducting carbon nanotubes. *Appl. Phys. Lett.*, 87, 172112.

[23] Saito, R., Dresselhaus, G., & Dresselhaus, M. S. (1998). Physical Property of Carbon Nanotubes. Imperial College Press London

[24] Suzuura, H., & Ando, T. (2002). Phonons and electron-phonon scattering in carbon nanotubes. *Phys. Rev. B*, 65, 235412.

[25] Goupalov, S. V. (2005). Continuum model for long-wavelength phonons in twodimensional graphite and carbon nanotubes. *Phys. Rev. B*, 71, 085420.

[26] Kurti, J., Kresse, G., & Kuzmany, H. (1998). First-principles calculation of the radial-breathing mode of single-wall carbon nanotubes. Phys. Rev. B. , 58, R8869.

[27] Sanchez, D., Portal, E., Artacho, J. , Soler, M., Rubio, A., & Ordejon, P. (1999). Ab initio structural, elastic, and vibrational properties of carbon nanotubes. *Phys. Rev. B*, 59, 12678.

[28] Dubay, O., & Kresse, G. (2003). Accurate density functional calculations for the phonon dispersion relations of graphite layer and carbon nanotubes. *Phys. Rev. B.*, 67, 035401.

[29] Mahan, G. D. (2003). Electron-optical phonon interaction in carbon nanotubes. *Phys. Rev. B*, 68, 125409.

[30] Jiang, J., Saito, R., Ge, G., Samsonidze, S. G., Chou, A., Jorio, G., & Dresselhaus, M. S. (2005). Electron-phonon matrix elements in single-wall carbon nanotubes. *Phys. Rev. B*, 72, 235408.

[31] Popov, V. N., & Lambin, P. (2006). Intraband electron-phonon scattering in single-walled carbon nanotubes. *Phys. Rev. B*, 74, 075415.

[32] Machon, M., Reich, S., Telg, H., Maultzsch, J., Ordejon, P., & Thomsen, C. (2005). Strength of radial breathing mode in single-walled carbon nanotubes. Phys. Rev. B. , 71, 035416.

[33] Guo, J. (2005). A quantum-mechanical treatment of phonon scattering in carbon nanotube transistors. *J. Appl. Phys.*, 98, 063519.

[34] Pourfath, M., Kosina, H., & Selberherr, S. (2006). Rigorous modeling of carbon nanotube transistors. *J. Phys.: Conf. Ser.*, 38, 29.

[35] Koswatta, S. O., Sayed, Hasan., Mark, S., Lundstrom, M. P., Anantram, Dmitri. E., & Nikonov, . (2007). Non-equilibrium Green's function treatment of phonon scattering in carbon nanotube transistors. *IEEE Trans. Elec. Dev.*, 54, 2339-2351.

[36] Dresselhaus, M. S., Dresselhaus, G., & Eklund, P. C. (1995). Science of Fullerenes and Carbon Nanotubes: Their Properties and Applications. *(Academic Press, Inc.)*, 0-12221-820-5.

[37] Kane, L., Mele, E. J., Lee, R. S., Fischer, J. E., Petit, P., Dai, H., Thess, A., Smalley, R. E., Verschueren, A. R. M., Tans, S. J., & Dekker, C. (1998). Temperature-dependent resistivity of single-wall carbon nanotubes. *Europhys. Lett.*, 41, 683-688.

[38] Appenzeller, J., Martel, R., Avouris, P., Stahl, H., & Lengeler, B. (2001). Optimized contact configuration for the study of transport phenomena in ropes of single-wall carbon nanotubes. *Appl. Phys. Lett.*, 78, 3313.

[39] Chen, Y. F., & Fuhrer, M. S. (2005). Electric-field-dependent charge-carrier velocity in semiconducting carbon nanotubes. *Phys. Rev. Lett.*, 95, 236803.

[40] Avouris, P., Chen, Z. H., & Perebeinos, V. (2007). Carbon-based electronics. *Nature Nanotech.*, 2, 605-615.

[41] Guo, J. (2005). A quantum-mechanical treatment of phonon scattering in carbon nanotube transistors. *J. Appl. Phys.*, 98, 063519.

[42] Guo, J., & Lundstrom, M. (2005). Role of phonon scattering in carbon nanotube field-effect transistors. *Appl. Phys. Lett.*, 86, 193103.

[43] John, L., Castro, L. C., Clifford, J. P., & Pulfrey, D. L. (2003). Electrostatics of coaxial schottky-barrier nanotube field-effect transistors. *IEEE Trans. Nanotech.*, 2, 175-180.

[44] Pennington, G., & Goldsman, N. (2003). Semi-classical transport and phonon scattering on electrons in semiconducting carbon nanotubes. *Phys. Rev. B.*, 68, 045426.

[45] Alam, K., & Lake, R. (2005). Performance of 2 nm gate length carbon nanotube field-effect transistors with source-drain underlaps. *Appl. Phys. Lett.*, 87, 073104.

[46] Verma Kauser, M. Z., & Ruden, P. P. (2005). Ensemble Monte Carlo transport simulations for semiconducting carbon nanotubes. *J. Appl. Phys.*, 97, 114319.

[47] Xia, T. S., Register, L. R., & Banerjee, S. K. (2004). Calculations and applications of the complex band structure for carbon nanotube field-effect transistors. Phys. Rev. B. , 70, 045332.

[48] Svizhenko Anantram, M. P. (2005). Effect of scattering and contacts on current and electrostatics in carbon nanotubes. *Phys. Rev. B.*, 72, 085430.

[49] Martel, R., Schmidt, T., Shea, H. R., Hertel, T., & Avouris, P. (1999). *Single- and Multi-Wall Carbon Nanotube*.

[50] Field-Effect Transistors,. (1998). *Appl. Phys. Lett.*, 73, 2447.

[51] Appenzeller, J., Knoch, J., Derycke, V., Martel, R., Wind, S., & Avouris, P. (2002). Field-Modulated Carrier Transport in Carbon Nanotube Transistors. *Phys. Rev. Lett.*, 89, 126801.

[52] Bardeen, J., & Shockley, W. (1950). Deformation Potentials and Mobilities in Non-Polar Crystals. *Phys. Rev.*, 80, 72.

[53] Beleznay, F. B., Bogar, F., & Ladik, J. (2003). Calculation of the charge-carrier mobility of polyguanylic acid: The simultaneous effect of stretching and twisting,. *J. Chem. Phys.*, 119, 5690.

[54] Long, M. Q., Tang, L., Wang, D., Wang, L. J., & Shuai, Z. G. (2009). Theoretical predictions of size dependent carrier mobility and polarity in graphene. *J. Am. Chem. Soc.*, 131, 177728-177731.

[55] Sa, N., Wang, G., Yin, B., & Huang, Y. (2008). Theoretical study on non-covalent functionalization of armchair carbon nanotube by tetrathiafulvalene molecule. Physica E. , 40, 2396-2399.

[56] Kresse, G., & Furthmüller, J. (1996). Efficiency of ab-initio total energy calculations for metals and semiconductors using a plane-wave basis set. *Comput. Mater. Sci.*, 6, 15.

[57] Kresse, G., & Furthmüller, J. (1996). Efficient iterative schemes for ab initio total-energy calculations using a plane-wave basis set, Phys. *Rev. B.*, 54, 11169.

[58] Perdew, J. P., Burke, K., & Ernzerhof, M. (1996). Generalized gradient approximation made simple. *Phys. Rev. Lett.*, 77, 3865.

[59] Blöchl, P. E. (1994). Projector augmented-wave method. Phys. Rev. B, , 50, 17953.

[60] Kresse, G., & Joubert, D. (1999). From ultrasoft pseudopotentials to the projector augmented-wave method. *Phys. Rev. B.*, 59, 1758.

[61] Sreekala, S., Peng, X. H., Ajayan, P. M., & Nayak, S. K. (2008). Effect of strain on the band gap and effective mass of zigzag single-wall carbon nanotubes: First-principles density-functional calculations. *Phys. Rev. B.*, 77, 155434.

[62] Xu, Y. D., Xia, J., Yin, X. G., Wan, K., Jiang, A. D., Li, D., Wu, Z. G., & Liu, . (2010). The effect of acoustic phonon scattering on the carrier mobility in the semiconducting zigzag single wall carbon nanotubes. *Appl. Phys. Lett.*, 96, 183108.

IntechOpen